CEVAR: Centerline Embedding Extraction for Endovascular Aneurysm Repair

Roman Naeem[1][0009-0001-2625-125X], Timo Niiniskorpi[2][0009-0008-7139-9430], Charlotte Sandström[2][0000-0002-6019-931X], Naman Desai[1][0009-0005-4296-9287], Ida Häggström[1][0000-0001-9178-6683], Fredrik Kahl[1][0000-0001-9835-3020], Håkan Roos[2][0000-0002-7838-1400], and Jennifer Alvén[1][0000-0003-4195-9325]

[1] Chalmers University of Technology, 412 96 Gothenburg, Sweden
[2] The University of Gothenburg, 405 30 Gothenburg, Sweden
nroman@chalmers.se

Abstract. Long-term mortality rates after endovascular aneurysm repair (EVAR) remain elevated due to post-EVAR rupture caused by loss of seal in stent graft sealing zones. Structured CT review using centerline measurements improves detection, but current workflows require manual centerline editing and expert operators. We propose CEVAR, a transformer framework for automated, protocol-driven sealing zone assessment that combines 3D centerline tracking with embedding-based geometric prediction. Two state-of-the-art image-to-graph models are evaluated for aorto-iliac centerline extraction from follow-up CT and for measurement of stent position, vessel diameters, and seal lengths according to EVAR4C protocol. Across the full test set and a challenging non-contrast subset, the proposed fully automatic method outperforms the commercial semi-automatic workflow. Code and pretrained models are available at https://github.com/RomStriker/CEVAR.

Keywords: Endovascular aneurysm repair (EVAR) · Vascular centerline extraction · 3D image-to-graph

1 Introduction

Abdominal aortic aneurysm is a dilation of the abdominal aorta exceeding 50% of normal diameter [9]. Enlargement increases rupture risk and treatment is recommended beyond a threshold size [23]. Endovascular Aneurysm Repair (EVAR) is now the predominant treatment due to favorable short term outcomes, yet long term survival remains limited due to late post-EVAR rupture [16].

Post-EVAR rupture is strongly associated with progressive loss of seal in proximal or distal stent graft sealing zones [5]. Structured follow-up protocols detect loss of seal in up to 40% of patients within five years and predict failure more reliably than aneurysm sac expansion or endoleaks [18].

The EVAR4C protocol [18] evaluates sealing zones using vessel centerlines as reference for length and orthogonal diameter measurements. It more than doubles the detection of seal loss compared to conventional review, but requires manual centerline editing by highly trained operators [2, 18].

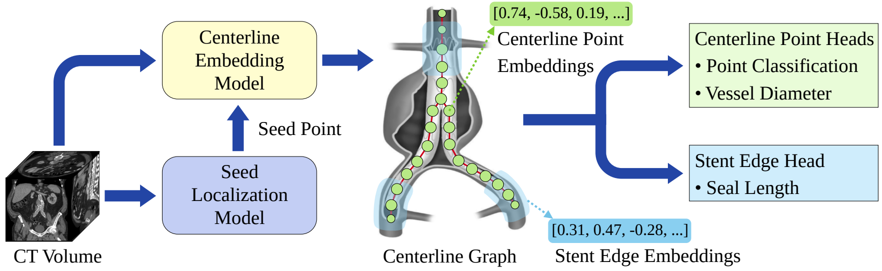

Fig. 1. Proposed CEVAR pipeline for automated post-EVAR analysis from CT. A seed point localized above the stent's proximal edge initializes a Transformer-based centerline model, which outputs the aorto-iliac centerline as point-wise embeddings; we evaluate both Trexplorer Super and RefTr, and extend RefTr with the prediction heads. Larger points lie inside the stent graft. The embeddings feed heads that classify each point as inside or outside the stent and predict vessel diameters, while a stent edge embedding aggregated at each graft edge predicts sealing-zone length.

Accurate centerline generation is a major bottleneck. Existing tools are designed for contrast-enhanced preoperative CT and require extensive manual adjustment [1, 4] in post-EVAR scans affected by metal artifacts, altered anatomy, and low contrast.

Prior deep learning for EVAR imaging has targeted screening [20], endoleak detection [24], morphological change [10], migration [3], and risk stratification [12], but these approaches detect late manifestations of failure without quantifying sealing zone integrity. Earlier centerline extraction work [17] produces segmentations rather than protocol measurements. To our knowledge, no previous study has used learned centerline embeddings for automated sealing zone quantification in post-EVAR CT.

Full automation of the EVAR4C protocol would enable standardized, objective sealing-zone evaluation in routine follow-up, reducing operator dependency and manual workload. We propose CEVAR, a fully automatic pipeline comprising seed localization, Transformer-based centerline embedding extraction, and embedding-based prediction heads for EVAR4C measurements, as illustrated in Fig. 1. Our key contributions are:

– CEVAR, a fully automatic, protocol-driven pipeline requiring no manual initialization, in which the point-wise embeddings produced during centerline tracking are reused directly to regress stent-edge location, vessel diameters, and seal length, rather than recovering these by geometric post-processing on the extracted curve.
– A systematic assessment of Transformer-based 3D centerline extraction in post-EVAR CT, addressing the challenges of metal artifacts and low contrast, including a quantitative comparison against a commercial semi-automatic workflow.
– A curated clinical dataset featuring manually refined centerlines and expert annotations for stent edges and sealing-zone measurements.

Taken together, this is primarily an application and translation study: the centerline model is adopted from prior work, and the contribution lies in assembling and validating a complete pipeline for a protocol-driven clinical task.

2 Method

The EVAR4C protocol specifies centerline-based measurements along the stent graft: vessel diameters at the graft edges and at 10 and 15 mm inward, and sealing-zone lengths measured along the centerline.

2.1 Datasets

Private Dataset. The dataset was collected retrospectively from a clinical cohort of patients treated with standard bifurcated EVAR at two hospitals during 2010-2012. Ethical approval was granted (508-14). For each patient, the preoperative CT, the postoperative CT at one month, the postoperative CT at one year, and the last available follow-up CT were reviewed. For each CT examination, centerlines were generated and subsequently manually adjusted by the reviewing physician using the commercially available software TeraRecon Intuition [21]. Stent-graft edge markers were placed manually, and all annotations followed the EVAR4C protocol. These grafts span device platforms still in widespread clinical use (e.g., Gore Excluder, Medtronic Endurant, Cook Zenith). Centerlines and sealing-zone annotations were double-evaluated, with most cases reviewed by two or more investigators. A separate inter-observer study was not performed, as the aortic centerline follows an unambiguous anatomical landmark with inherently low inter-rater variability.

To train the centerline extraction models, we utilized 374 scans from 142 subjects, partitioned by subject into training, validation, and test sets. The training set contains 267 scans (102 subjects; 207 contrast/60 non-contrast), the validation set 32 scans (12 subjects; 30 contrast/2 non-contrast), and the test set 75 scans (28 subjects; 59 contrast/16 non-contrast).

Aorta24 Centerline Dataset. We derived a centerline dataset from the public Aorta24 challenge [7], which consists of 100 CT scans with corresponding multi-class aorta segmentation masks. Centerlines were automatically extracted from these masks using the Vascular Modeling Toolkit (VMTK) [8, 19] and served as the foundation for pretraining the centerline models.

The Aorta24 license precludes redistributing derived annotations, so the extraction script is shared rather than the centerlines themselves; the private clinical dataset is governed by ethical permission and is being actively expanded, preventing immediate public release.

2.2 Centerline Extraction Methods

We compare the commercial postprocessing workflow with state-of-the-art deep learning-based image-to-graph centerline extraction methods.

TeraRecon Intuition. TeraRecon Intuition [21] is a standard commercial platform for radiological post-processing. Its dedicated EVAR workflow uses an intensity-guided algorithm that assumes sufficient contrast enhancement for vessel tracking, linking user-defined markers based on local voxel intensities. We evaluate three initialization modes, relabeled by seed count for clarity: SemAuto, in which the user selects the correct left and right centerlines from automatically generated candidate paths, and 2Seeds and 4Seeds, in which the user marks two or four points bounding the aorto-iliac branches.

Trexplorer Super. Trexplorer Super [13] is an image-to-graph framework using a Transformer architecture [15, 22] to extract vascular centerline graphs from CT volumes via sequential tracking. From a localized seed point, it expands the centerline graph breadth-first into a topologically consistent tree without disconnected components or cycles. A recursive tracking module autoregressively predicts the next point embedding from the current one, capturing local image features and long-range spatial dependencies along the vessel lumen. A multi-class classification head labels embeddings as intermediate, bifurcation, end, or background, terminating tracking and spawning new branches at bifurcations while preserving global connectivity.

RefTr. RefTr [14] is a parameter-efficient 3D image-to-graph model representing centerline trees as confluent trajectories that share a root and follow the same path until bifurcation. Using a Transformer-based Producer–Refiner architecture, the Producer generates candidate trajectories from the input patch root at its center, and a shared Refiner iteratively aligns them with the target branches. This approach refines entire trajectories while enforcing topologically valid tree structures, improving precision and making the model lighter and faster than Trexplorer Super. RefTr predicts multiple candidates per target, creating an ensembling effect resolved by a novel Tree Non-Maximum Suppression (TNMS) that merges redundant branches while preserving global topology. It also extends Trexplorer Super's evaluation framework, adding radius-aware thresholds to its point-, branch-, and graph-level metrics, which we adopt in this work.

Prediction Heads. Due to RefTr's superior efficiency and performance, we extend it to predict EVAR4C protocol measurements. Beyond the standard centerline embedding heads, we add:

1. **Stent point classification head:** A binary head that predicts whether each centerline point lies inside or outside the stent. Stent edges are localized as the points where this label transitions, giving the proximal and the two distal edges. At these edge points, the radii at the edge and at 10 mm and 15 mm inward are obtained by fine-tuning the pretrained radius head on the corresponding point embeddings. We convert the radii to diameters to match the EVAR4C protocol.

2. **Stent edge token and regression head:** Seal length is a property of a segment rather than of a single point, so it cannot be attributed to one centerline embedding. When an edge is detected within a sub-volume, we introduce an additional learned stent edge token that aggregates information across the surrounding point embeddings, together with a regression head that predicts seal length from it. The same token and head are also evaluated for the three diameters, allowing the two prediction heads to be compared.

Automatic Seed Localization. To enable a fully automated post-EVAR analysis pipeline, we replace manual initialization with a learned seed localization module. A pretrained SwinUNETR [6] was fine-tuned for 80,000 iterations to regress a heatmap centered on the stent's proximal edge. The peak of the thresholded heatmap gives the edge location, and the seed is placed 10 mm proximal to it so that tracking begins with context above the graft.

Training Strategy. Trexplorer Super and RefTr were pretrained on the Aorta24 centerline dataset for 2 million iterations. These pretrained weights initialized all subsequent fine-tuning experiments on the private dataset, with each model fine-tuned for 200,000 iterations. Training used a cosine annealing learning rate scheduler with a single 20,000-iteration warm-up at the start and a base learning rate of 7×10^{-4}, on a single NVIDIA RTX A6000 GPU (48 GB VRAM) with a batch size of 8. Pretraining and fine-tuning required 190/21 and 124/14 GPU hours for Trexplorer Super and RefTr, respectively.

3 Experiments and Results

3.1 Evaluation Metrics

For centerline evaluation, we adopt the hierarchical metrics proposed in RefTr [14]. Node-level performance is measured using radius-aware Average Precision (rAP), Recall (rAR), and F1-score ($rF1$). A predicted node is considered a true positive (TP) if it lies within a radius τ^{rad} of an unmatched target node. Inspired by the standard mAP/mAR formulation [11], these metrics are averaged over $\tau^{rad} \in [3.0, 15.0]$ mm with a 1.5 mm step for scale-robust localization; as vessel diameters span 7.6–56.5 mm, no single radius threshold is representative.

Branch-level metrics ($rBAP$, $rBAR$, $rBF1$) evaluate structural connectivity, where a branch is a TP if it covers at least a fraction τ^{match} of nodes from an unmatched target branch. These are averaged over $\tau^{match} \in [0.4, 0.8]$ with a 0.05 step, using $\tau^{rad} = 6.0$ mm. Predictions outside the stent region are discarded, as the ground truth centerline is not well-defined in these areas. Graph-level topology is assessed using the Mean Absolute Error (MAE) of Betti-0 (connected components) and Betti-1 (cycles) numbers. We also report MAE in mm for vessel diameter and seal length. The centerline models predict vessel radii, whereas the EVAR4C protocol specifies diameters; all diameter errors are therefore computed after converting predicted radii to diameters.

Table 1. Point-level and branch-level results for centerline extraction on the **full test set**. TeraRecon (TR) is evaluated under three seeding strategies (SemAuto, 2Seeds, 4Seeds), and Trexplorer Super (Trex), Trexplorer Super with Tree Non-maximum Suppression (TrexTNMS), and RefTr under single-seed (1Seed) and fully automatic (Auto) initialization. All Auto rows use our seed localization module in place of a manual seed and differ only in the centerline extraction method. Best values in bold.

Model	Point-level@ $\tau^{\mathrm{rad}} = [3.0{:}1.5{:}15.0]\ mm$			Branch-level@ $\tau^{\mathrm{match}} = [0.4{:}0.05{:}0.8]$		
	rAP(%)↑	rAR(%)↑	rF1(%)↑	rBAP(%)↑	rBAR(%)↑	rBF1(%)↑
Commercial Semi-automatic Methods						
TR:SemAuto	2.0	2.4	2.1	2.7	2.3	2.4
TR:2Seeds	53.5	58.6	55.2	71.9	60.6	63.9
TR:4Seeds	60.3	66.1	62.6	76.8	66.3	68.9
Centerline Semi-automatic Methods (1Seed)						
Trex	68.6 ± 1.1	72.4 ± 1.1	69.1 ± 0.2	89.8 ± 1.0	80.6 ± 2.5	83.3 ± 1.2
TrexTNMS	71.3 ± 1.0	73.0 ± 1.8	70.8 ± 0.3	94.3 ± 1.3	80.0 ± 2.0	84.6 ± 0.4
RefTr	70.5 ± 0.2	**78.5 ± 0.6**	73.3 ± 0.3	**94.5 ± 0.9**	**85.5 ± 0.9**	**88.5 ± 0.4**
Centerline Fully Automatic Methods (Auto)						
Trex	74.8 ± 1.7	71.5 ± 0.9	71.3 ± 0.7	89.1 ± 2.4	59.4 ± 0.7	68.6 ± 0.3
TrexTNMS	**78.5 ± 1.4**	72.5 ± 2.0	73.6 ± 0.4	94.5 ± 2.3	60.2 ± 1.2	70.3 ± 0.7
RefTr	76.1 ± 0.3	75.7 ± 0.9	**74.6 ± 0.7**	93.8 ± 0.8	66.2 ± 1.1	75.2 ± 0.7

Table 2. Point-level and branch-level results for centerline extraction on the **non-contrast test set**. TeraRecon (TR), Trexplorer Super (Trex), Trexplorer Super with Tree Non-maximum Suppression (TrexTNMS), and RefTr are evaluated as in Table 1.

Model	Point-level@ $\tau^{\mathrm{rad}} = [3.0{:}1.5{:}15.0]\ mm$			Branch-level@ $\tau^{\mathrm{match}} = [0.4{:}0.05{:}0.8]$		
	rAP(%)↑	rAR(%)↑	rF1(%)↑	rBAP(%)↑	rBAR(%)↑	rBF1(%)↑
Commercial Semi-automatic Methods						
TR:SemAuto	0.0	0.0	0.0	0.0	0.0	0.0
TR:2Seeds	4.9	4.1	4.1	7.4	4.2	4.9
TR:4Seeds	15.2	13.6	14.2	25.7	13.2	13.2
Centerline Semi-automatic Methods (1Seed)						
Trex	66.9 ± 1.9	60.3 ± 4.5	62.3 ± 2.7	90.3 ± 3.6	66.4 ± 7.7	73.2 ± 7.2
TrexTNMS	68.5 ± 1.4	60.8 ± 4.8	63.4 ± 3.0	**91.2 ± 4.1**	66.7 ± 7.5	**73.8 ± 7.3**
RefTr	58.4 ± 2.2	59.9 ± 1.2	58.1 ± 0.6	83.0 ± 1.4	**69.2 ± 2.7**	73.0 ± 1.6
Centerline Fully Automatic Methods (Auto)						
Trex	76.3 ± 0.6	61.0 ± 1.8	66.6 ± 0.7	88.7 ± 2.8	46.5 ± 0.9	58.2 ± 1.0
TrexTNMS	**77.8 ± 0.5**	**62.0 ± 2.3**	**67.8 ± 1.2**	90.8 ± 1.7	47.7 ± 1.2	59.9 ± 0.8
RefTr	68.7 ± 2.7	61.0 ± 1.8	63.4 ± 0.6	85.3 ± 5.1	53.0 ± 1.0	62.6 ± 1.1

For stent node classification, we report mean Average Precision (mAP), mean Recall (mRec), and mean maximum F1-score (mF1), averaged across all τ^{rad} thresholds. All results reflect the mean and standard deviation across three independent runs.

Table 3. Accuracy of the sealing-zone measurements specified by the EVAR4C protocol, regressed directly from the point-wise centerline embeddings produced by the fully automatic RefTr configuration of Table 1. Two prediction heads are evaluated: the fine-tuned pretrained radius head, which provides only the diameters, and a new regression head operating on an additional learned stent edge token, which predicts the seal length as well. Diameters are measured at the proximal and the two distal stent edges, and at 10 and 15 mm inward from each edge. Best diameter values in bold.

Prediction head	Prox. Edge Diameter (MAE, mm)↓			Right Edge Diameter (MAE, mm)↓		
	Edge	@10 mm	@15 mm	Edge	@10 mm	@15 mm
Radius Finetuned	**1.3 ± 0.1**	**1.8 ± 0.1**	**2.1 ± 0.1**	**2.6 ± 0.1**	**1.8 ± 0.1**	**1.9 ± 0.1**
Stent Edge Token	1.6 ± 0.2	2.4 ± 0.1	2.7 ± 0.1	3.5 ± 0.4	3.3 ± 0.6	3.2 ± 0.7
Prediction head	**Left Edge Diameter (MAE, mm)↓**			**Stent Seal Length (MAE, mm)↓**		
	Edge	@10 mm	@15 mm	Proximal	Right	Left
Radius Finetuned	**2.1 ± 0.1**	**1.8 ± 0.1**	**2.2 ± 0.1**	–	–	–
Stent Edge Token	3.1 ± 0.2	2.9 ± 0.1	3.1 ± 0.2	9.1 ± 0.4	13.1 ± 0.5	11.9 ± 0.2

3.2 Results

Table 1 summarizes point- and branch-level performance on the full test set. Commercial semi-automatic extraction (TeraRecon, TR) required multiple seeds for reasonable accuracy and still trailed learning-based methods. Among single-seed approaches, RefTr performed best, with the highest point-level recall and F1 and the highest branch F1; applying Tree Non-max Suppression to Trexplorer Super (TrexTNMS) improved branch precision but lagged RefTr in recall. In the fully automatic setting, all learning-based methods outperformed the commercial baseline: TrexTNMS achieved the highest precision, while RefTr gave the best precision–recall balance (highest branch F1 and recall), indicating superior recovery of full vascular trees without manual initialization.

As shown in Table 2, on the non-contrast subset, the commercial method degraded severely, with near-zero scores even with additional seeds. Learning-based methods remained robust: TrexTNMS achieved the highest fully automatic point-level F1, and RefTr showed competitive branch recall.

For topology on the full test set, commercial extraction showed decreasing connectivity errors with more seeds (Betti-0 MAE: $0.960 \rightarrow 0.347 \rightarrow 0.027$), whereas all learning-based methods achieved perfect topology (Betti-0 = Betti-1 = 0). On non-contrast scans the commercial method again degraded (Betti-0 MAE: $0.938 \rightarrow 0.812 \rightarrow 0.063$), while learning-based approaches produced topologically correct trees in all modes.

Vessel diameters across proximal and distal stent edges ranged from roughly 7.6 to 56.5 mm, and seal lengths from 0 to 77.6 mm across sealing zones, reflecting substantial anatomical variability. Table 3 reports diameter and seal-length accuracy. Fine-tuning the pretrained radius head achieved the lowest diameter errors and is therefore used in CEVAR; the stent edge token enabled seal-length prediction, but at 9 to 13 mm the error is too large for clinical use and is reported as a feasibility result. Stent-region classification was strong across models (mAP

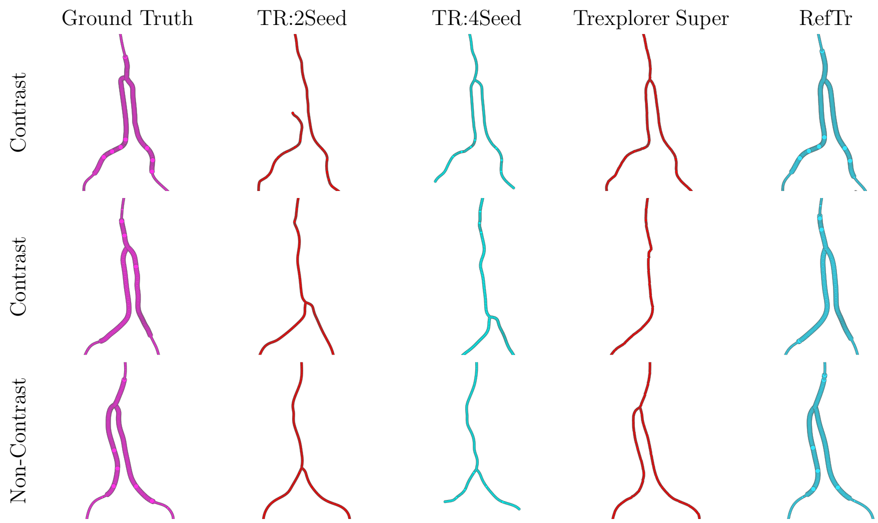

Fig. 2. Visual comparison of ground truth and predicted centerlines on two contrast-enhanced and one non-contrast test case. Larger points indicate stent nodes for the ground truth and RefTr, which uses a stent classification head. TR:SemAuto is omitted due to poor performance.

$= 0.860 \pm 0.003$, mRec $= 0.763 \pm 0.008$, mF1 $= 0.826 \pm 0.005$). Together, the accurate stent-region classification and the sub-2 mm proximal diameter errors obtained from the same point-wise embeddings indicate that these encode both local lumen scale and graft presence. The larger seal-length errors likely stem not from the aggregation, since the same token recovers diameters reasonably well, but from supervision: a single scalar per zone provides no per-point signal comparable to that for radius.

Fig. 2 shows qualitative examples. TeraRecon misses the aorto-iliac bifurcation location in all three cases and produces disconnected branches in the top row, consistent with its non-zero Betti-0 error; Trexplorer Super misses an iliac branch in the middle case, whereas RefTr recovers the complete bifurcated tree in all three, including the non-contrast case.

4 Discussion and Conclusion

CEVAR combines 3D centerline tracking with embedding-based geometric prediction for protocol-driven sealing-zone assessment. Compared to commercial semi-automatic software, it delivers substantially improved geometric accuracy and topological consistency, including on challenging non-contrast CT.

We benchmark against centerline-native methods rather than segmentation-plus-skeletonization: the EVAR4C protocol operates directly on centerline points, our cohort provides only centerline annotations, and downstream prediction consumes point-wise embeddings that skeletonization does not provide.

Accurate centerline extraction is a prerequisite for reliable sealing-zone evaluation under EVAR4C. Our results show that learning-based centerline tracking reduces dependence on manual adjustment while preserving the geometric consistency required downstream: the learned point-wise embeddings enable reliable identification of stent-graft edges and accurate diameter measurement.

Seal-length prediction is not yet accurate enough for clinical use, likely reflecting the difficulty of modeling interactions between the vessel and the stent, where separation of the wall from the graft is subtle. The cohort is also retrospective, drawn from two centers and a limited set of device platforms, with a test set of 75 scans from 28 subjects; generalization across scanners, reconstruction protocols, and graft designs, as well as external validation, remains to be established. Ongoing work therefore focuses on expanding the cohort and adding pixel-wise annotations of sealing-zone geometry. The framework also enables use of existing large-scale longitudinal follow-up data consisting of routine CT examinations with associated tabular measurements, opening the way to fully automated EVAR follow-up pipelines at substantially larger scale.

Acknowledgments. The compute resources were provided by the National Academic Infrastructure for Supercomputing in Sweden (NAISS), partially funded by the Swedish Research Council through grant agreement no. 2022-06725.

Disclosure of Interests. The authors have no competing interests to declare that are relevant to the content of this article.

References

1. Adam, C., Fabre, D., Mougin, J., Zins, M., Azarine, A., Ardon, R., d'Assignies, G., Haulon, S.: Pre-surgical and post-surgical aortic aneurysm maximum diameter measurement: full automation by artificial intelligence. European Journal of Vascular and Endovascular Surgery **62**(6), 869–877 (2021)
2. Andersson, M., Sandström, C., Stackelberg, O., Lundqvist, R., Nordanstig, J., Jonsson, M., Roy, J., Hultgren, R., Roos, H.: Structured computed tomography analysis can identify the majority of patients at risk of post-endovascular aortic repair rupture. Journal of Vascular Surgery **76**(5), 1424 (2022)
3. Asenbaum, U., Schoder, M., Schwartz, E., Langs, G., Baltzer, P., Wolf, F., Prusa, A.M., Loewe, C., Nolz, R.: Stent-graft surface movement after endovascular aneurysm repair: baseline parameters for prediction, and association with migration and stent-graft-related endoleaks. European Radiology **29**(12), 6385–6395 (2019)
4. Corriere, M.A., Islam, A., Craven, T.E., Conlee, T.D., Hurie, J.B., Edwards, M.S.: Influence of computed tomography angiography reconstruction software on anatomic measurements and endograft component selection for endovascular abdominal aortic aneurysm repair. Journal of Vascular Surgery **59**(5), 1224–1231 (2014)
5. Gonçalves, F.B., Oliveira, N., Van Rijn, M.J., Ultee, K., Hoeks, S., Ten Raa, S., Stolker, R., Verhagen, H.: Iliac seal zone dynamics and clinical consequences after endovascular aneurysm repair. European Journal of Vascular and Endovascular Surgery **53**(2), 185–192 (2017)

6. Hatamizadeh, A., Nath, V., Tang, Y., Yang, D., Roth, H.R., Xu, D.: Swin unetr: Swin transformers for semantic segmentation of brain tumors in mri images. In: International MICCAI brainlesion workshop. pp. 272–284. Springer (2021)
7. Imran, M., Krebs, J.R., Cooper, M.A., Ma, J., Zhou, Y., Shao, W.: Multi-class segmentation of the aorta. In: AortaSeg 2024 Challenge, Held in Conjunction with MICCAI 2024. Springer, Cham, Switzerland (2024). https://doi.org/10.1007/978-3-032-14246-7
8. Izzo, R., Steinman, D., Manini, S., Antiga, L.: The vascular modeling toolkit: A python library for the analysis of tubular structures in medical images. Journal of Open Source Software **3**(25), 745 (2018). https://doi.org/10.21105/joss.00745
9. Johnston, K.W., Rutherford, R.B., Tilson, M.D., Shah, D.M., Hollier, L., Stanley, J.C., et al.: Suggested standards for reporting on arterial aneurysms. Journal of vascular surgery **13**(3), 452–458 (1991)
10. Lareyre, F., Raffort, J., Kakkos, S.K., D'oria, M., Nasr, B., Saratzis, A., Antoniou, G.A., Hinchliffe, R.J.: Imaging analysis using artificial intelligence to predict outcomes after endovascular aortic aneurysm repair: protocol for a retrospective cohort study. BMJ open **15**(7), e098724 (2025)
11. Lin, T.Y., Maire, M., Belongie, S., Hays, J., Perona, P., Ramanan, D., Dollár, P., Zitnick, C.L.: Microsoft coco: Common objects in context. In: European conference on computer vision. pp. 740–755. Springer (2014)
12. Long, B., Cremat, D.L., Serpa, E., Qian, S., Blebea, J.: Applying artificial intelligence to predict complications after endovascular aneurysm repair. Vascular and Endovascular Surgery **58**(1), 65–75 (2024)
13. Naeem, R., Hagerman, D., Alvén, J., Svensson, L., Kahl, F.: Trexplorer super: Topologically correct centerline tree tracking of tubular objects in ct volumes. In: International Conference on Medical Image Computing and Computer-Assisted Intervention. pp. 595–605. Springer (2025)
14. Naeem, R., Hagerman, D., Alvén, J., Kahl, F.: Reftr: Recurrent refinement of confluent trajectories for 3d vascular tree centerlines (2026), https://arxiv.org/abs/2511.20823
15. Naeem, R., Hagerman, D., Svensson, L., Kahl, F.: Trexplorer: Recurrent detr for topologically correct tree centerline tracking. In: International Conference on Medical Image Computing and Computer-Assisted Intervention. pp. 744–754. Springer (2024)
16. Powell, J.T., Sweeting, M.J., Ulug, P., Blankensteijn, J.D., Lederle, F., Becquemin, J., Greenhalgh, R., Greenhalgh, R., Beard, J., Buxton, M., et al.: Meta-analysis of individual-patient data from evar-1, dream, over and ace trials comparing outcomes of endovascular or open repair for abdominal aortic aneurysm over 5 years. Journal of British Surgery **104**(3), 166–178 (2017)
17. Sabrowsky-Hirsch, B., Thumfart, S., Fenz, W., Hofer, R., Schmit, P., Fellner, F.: Automatic segmentation of the abdominal aorta and stent-grafts. Journal of Image and Graphics **9**(3) (2021)
18. Sandström, C., Andersson, M.B., Bogdanovic, M., Fattahi, N., Lundqvist, R., Andersson, M., Roy, J., Hultgren, R., Roos, H.: Sealing zone failure decreases the long term durability of endovascular aneurysm repair. European Journal of Vascular and Endovascular Surgery **69**(2), 238–247 (2025). https://doi.org/10.1016/j.ejvs.2024.09.007
19. Slicer Development Community: 3d slicer. https://www.slicer.org/ (2025), accessed: 2026-02-20

20. Spinella, G., Fantazzini, A., Finotello, A., Vincenzi, E., Boschetti, G.A., Brutti, F., Magliocco, M., Pane, B., Basso, C., Conti, M.: Artificial intelligence application to screen abdominal aortic aneurysm using computed tomography angiography. Journal of Digital Imaging **36**(5), 2125–2137 (2023)
21. TeraRecon, Inc.: Intuition advanced visualization platform. Computer software (2025), https://www.terarecon.com
22. Vaswani, A., Shazeer, N., Parmar, N., Uszkoreit, J., Jones, L., Gomez, A.N., Kaiser, Ł., Polosukhin, I.: Attention is all you need. Advances in neural information processing systems **30** (2017)
23. Wanhainen, A., Van Herzeele, I., Bastos Goncalves, F., Bellmunt Montoya, S., Berard, X., Boyle, J.R., D'Oria, M., Prendes, C.F., Karkos, C.D., Kazimierczak, A., Koelemay, M.J., Kölbel, T., Mani, K., Melissano, G., Powell, J.T., Trimarchi, S., Tsilimparis, N., Antoniou, G.A., Björck, M., Coscas, R., Dias, N.V., Kolh, P., Lepidi, S., Mees, B.M., Resch, T.A., Ricco, J.B., Tulamo, R., Twine, C.P., Branzan, D., Cheng, S.W., Dalman, R.L., Dick, F., Golledge, J., Haulon, S., van Herwaarden, J.A., Ilic, N.S., Jawien, A., Mastracci, T.M., Oderich, G.S., Verzini, F., Yeung, K.K.: Editor's choice – european society for vascular surgery (esvs) 2024 clinical practice guidelines on the management of abdominal aorto-iliac artery aneurysms. European Journal of Vascular and Endovascular Surgery **67**(2), 192–331 (2024). https://doi.org/10.1016/j.ejvs.2023.11.002
24. Yang, Q., Hu, J., Luo, Y., Jia, D., Chen, N., Yao, C., Wu, R.: Detection of endoleak after endovascular aortic repair through deep learning based on non-contrast ct. CardioVascular and Interventional Radiology **47**(9), 1267–1275 (2024)